CHAPTER 4

SYNTHESIS AND CHARACTERIZATION OF Li_2O–(2-3x)MgO–(x)Al_2O_3–P_2O_5 (LMAP) CERAMIC FOR LTCC APPLICATION

4.1 Introduction

There are many ceramic materials with excellent microwave dielectric properties. However, these materials generally have high sintering temperatures [Sebastian et al. (2015)]. Low sintering temperature is required for co-firing the ceramic with the electrode material. Low temperature co-fired ceramics (LTCC) technology enables the fabrication of three dimensional ceramic modules with embedded silver or gold electrodes [Sebastian et al. (2015)]. Silver is the most commonly used electrode material. The material requirements for LTCC applications are described in detail in Chapter 1. In recent years, many researchers have found various materials with low sintering temperature (<1000 ^oC) and matching coefficient of thermal expansion with other co-firing materials for integration with miniaturized microwave devices [Thomas et al. (2013)]. Also, only a handful of ultra-low temperature co-fired ceramic (ULTTC) materials with sintering temperatures less than 700 ^oC are developed [Joseph et al. (2016); Varghese et al. (2016); Suresh et al. (2016); Induja et al. (2017)].

There are various methods to lower the sintering temperature of ceramics described in the Chapter 1. To lower the sintering temperature, generally glass with low softening temperature is added to the ceramic systems. However, the addition of glass increases the loss tangent of the composite due to presence of network formers in the glasses. The microwave energy is possibly absorbed by the network formers [Sebastian et al. (2016)]. There are two approaches to develop glass based LTCC materials i.e. glass-ceramic and glass + ceramic routes. The densification is achieved through controlled crystallization in

glass-ceramics [Sebastian et al. (2008b, 2015)] and liquid phase sintering in glass + ceramic routes [Sasikala et al. (2008); Manu et al. (2011); Varghese et al. (2013); Arun et al. (2017)] respectively. The commercially available LTCC materials are generally glass-ceramic or glass + ceramic materials. Recently, emphasis is given on the development of glass free ceramic systems to achieve good microwave dielectric properties with low loss and a small number of investigations have been reported for glass free ceramic systems with low sintering temperature [Joseph et al. (2016); Suresh et al. (2016); Bian et al. (2012, 2014); Valant et al. (2004); Thomas and Sebastian (2010, 2012); Sebastian et al. (2008a)].

The $LiMgPO_4$ ceramic system has been reported previously as a suitable LTCC material. Many researchers have studied this system by replacing Mg^{2+} with various transition metal elements like Zn, Cu, Ni, Co in different proportions [Thomas et al. (2010, 2012); Sebastian et al. (2008a); Dong et al. (2014b, 2014c)]. Investigations on $LiMg_{(1-x)}A_xPO_4$ ceramic (with A = Zn^{+2}, Co^{+2}, Ni^{+2}) shows good microwave dielectric properties and chemical compatibility with electrode material, silver. Dong et al. (2014a) have studied $Ba_3(VO_4)_2$–$LiMgPO_4$ composite ceramics with good microwave dielectric properties and low sinterability temperature down to 850 ^oC.

Low sintering temperature material with good microwave dielectric properties can be utilized for microwave device applications like filters, couplers, diplexers, microstrip antennas and dielectric resonator antennas [Ullah et al. (2015); Kumari and Gangwar (2016); Kumar and Gupta (2013); Balanis (2005); Petosa (2007); Luk and Leung (2003)].

4.2 Material synthesis

Li_2O–$(2-3x)MgO$–$(x)Al_2O_3$–P_2O_5 (LMAP) ceramics with x = (0.00 – 0.08) were prepared by solid state route. In each case approximately 25 g of chemical constituents were taken as batch composition and all the chemicals used were of high purity grade (Sigma Aldrich

and Alfa Aesar) with > 99% purity. The synthesis steps have been discussed in section 3.1.2 of Chapter 3. Thermal reaction and decomposition behaviour of different batch compositions were studied using TGA/DTA machine within the temperature range 30 – 1000 ^{o}C using a heating rate of 5 ^{o}C/min in argon atmosphere. The powders were pressed uni-axially to form cylindrical (diameter = 12mm, thickness = 2mm) and rectangular (length = 23mm, width = 11mm, height = 2 – 3 mm) pellets. All pellets were sintered in the temperature range 800 – 925 ^{o}C with a heating and cooling rate of 2 ^{o}C per minute. The bulk density of the sintered pellets was determined by Archimedes principle. Maximum densification achieved at 825 ^{o}C for the LMAP samples with x = 0.02 to 0.08. For the pure sample (x = 0), the densification increases with the increase in sintering temperature up to 925 ^{o}C. It was also reported in the previous study that the maximum density for $LiMgPO_4$ ceramic is achieved at 950 ^{o}C and above this temperature the densification further decreases [Thomas et al. (2010)]. All the pellets were sintered at optimized sintering temperature of 825 ^{o}C for 6 h. The formula for different batches is given in Table 4.1 and the compositions of different LMAP batches are tabulated in Tables 4.2 to 4.6.

Table 4.1 Different LMAP batch compositions

x	**Formula**
0.00	$Li_2O–2MgO–P_2O_5$
0.02	$Li_2O–1.94MgO–0.02Al_2O_3–P_2O_5$
0.04	$Li_2O–1.88MgO–0.04Al_2O_3–P_2O_5$
0.06	$Li_2O–1.82MgO–0.06Al_2O_3–P_2O_5$
0.08	$Li_2O–1.76MgO–0.08Al_2O_3–P_2O_5$

Table 4.2 Batch composition for $Li_2O–2MgO–P_2O_5$

Compound Name	Mol. Wt.	Purity (%)	Fraction	Mol. Wt. *fraction	Wt. %	Assay Correction	For 25 g
Li_2CO_3	73.89	99	0.5	36.9450	19.2147	19.4088	4.8037
MgO	40.3	99	1	40.3000	20.9596	21.1713	5.2399
Al_2O_3	101.96	99.5	0	0	0.0000	0.0000	0.0000
$NH_4H_2PO_4$	115.03	99	1	115.0300	59.8258	60.4301	14.9564
Total				192.2750	100.0000	101.0101	25.0000

Table 4.3 Batch composition for $Li_2O–1.94MgO–0.02Al_2O_3–P_2O_5$

Compound Name	Mol. Wt.	Purity (%)	Fraction	Mol. Wt. *fraction	Wt. %	Assay Correction	For 25 g
Li_2CO_3	73.89	99	0.5	36.9450	19.2336	19.4279	4.8085
MgO	40.3	99	0.97	39.0910	20.3508	20.5564	5.0878
Al_2O_3	101.96	99.5	0.01	1.0196	0.5308	0.5335	0.1320
$NH_4H_2PO_4$	115.03	99	1	115.0300	59.8848	60.4897	14.9716
Total				192.0856	100.0000	101.0074	25.0000

Table 4.4 Batch composition for $Li_2O–1.88MgO–0.04Al_2O_3–P_2O_5$

Compound Name	Mol. Wt.	Purity (%)	Fraction	Mol. Wt. *fraction	Wt. %	Assay Correction	For 25 g
Li_2CO_3	73.89	99	0.5	36.9450	19.2526	19.4471	4.8134
MgO	40.3	99	0.94	37.8820	19.7409	19.9403	4.9355
Al_2O_3	101.96	99.5	0.02	2.0392	1.06266	1.0680	0.2643
$NH_4H_2PO_4$	115.03	99	1	115.0300	59.9439	60.5494	14.9868
Total				191.8962	100.0000	101.0047	25.0000

Table 4.5 Batch composition for $Li_2O–1.82MgO–0.06Al_2O_3–P_2O_5$

Compound Name	Mol. Wt.	Purity (%)	Fraction	Mol. Wt. *fraction	Wt. %	Assay Correction	For 25 g
Li_2CO_3	73.89	99	0.5	36.9450	19.2716	19.4663	4.8183
MgO	40.3	99	0.91	36.6730	19.1297	19.3230	4.7828
Al_2O_3	101.96	99.5	0.03	3.0588	1.5956	1.6036	0.3969
$NH_4H_2PO_4$	115.03	99	1	115.0300	60.0031	60.6092	15.0020
Total				191.7068	100.0000	101.0020	25.0000

Table 4.6 Batch composition for Li_2O–1.76MgO–0.08Al_2O_3–P_2O_5

Compound Name	Mol. Wt.	Purity (%)	Fraction	Mol. Wt. *fraction	Wt. %	Assay Correction	For 25 g
Li_2CO_3	73.89	99	0.5	36.9450	19.2907	19.4855	4.8232
MgO	40.3	99	0.88	35.4640	18.5174	18.7044	4.6298
Al_2O_3	101.96	99.5	0.04	4.0784	2.1295	2.1402	0.5298
$NH_4H_2PO_4$	115.03	99	1	115.0300	60.0624	60.6691	15.0172
Total				191.5174	100.0000	100.9993	25.0000

4.3 Results and discussion

4.3.1 Thermo-gravimetric and differential thermal analysis

Thermo-gravimetric (TG) and Differential thermal analysis (DTA) of LMAP ceramics were done with heating rate of 5 ^oC/min. Figure 4.1(a) and 4.1(b) show the TG and DTA plot for LMAP compositions respectively. In Figure 4.1(b), an endothermic peak is observed at 200 ^oC indicating the decomposition of lithium carbonate. Initially, a rapid weight loss of about 13 % was observed up to 200 ^oC followed by weight loss of 15 – 18 % up to 450 ^oC. The decomposition of lithium carbonate occurs at 157 ^oC [Shi et al. (2015)], and the melting point of ammonium orthophosphate is 190 ^oC [Lide (2007)] after which its decomposition starts. Thus, the major weight loss observed up to 200 ^oC is due to decomposition of ammonium orthophosphate and carbonate which produces ammonia and carbon dioxide. The burnout process is completed at 450 ^oC. Total weight loss of about 18 % was observed within the temperature range 30 – 450 ^oC. There was no further weight loss above 450 ^oC in the TG curve. It may be associated with the solid reaction process forming the crystal phase of $LiMgPO_4$ [Shi et al. (2015)].

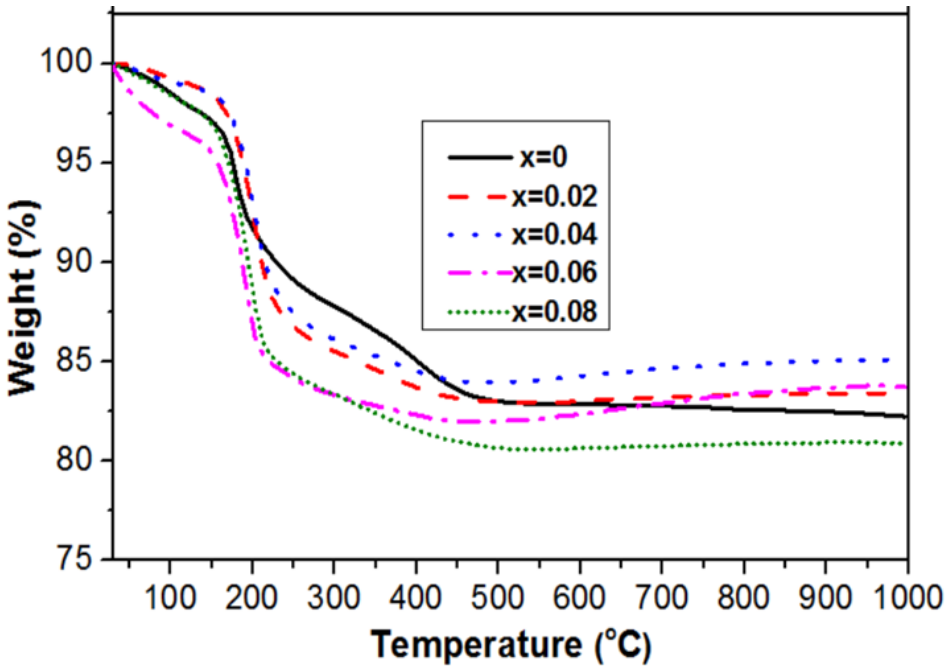

(a)

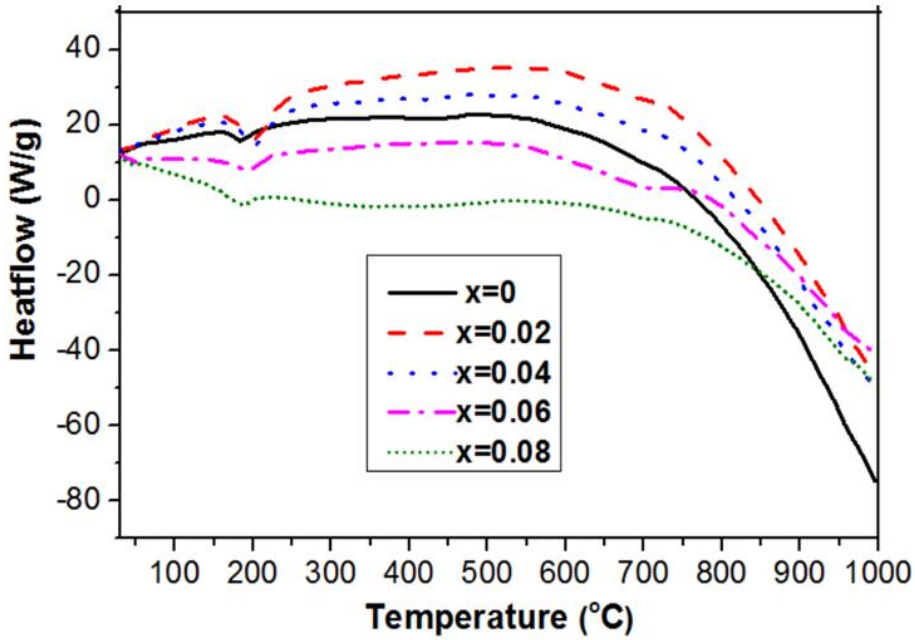

(b)

Figure 4.1 (a) TG plot and (b) DTA plot of LMAP ceramics.

Thus, the primary calcination temperature is taken as 500 ^{o}C followed by second calcination at 800 ^{o}C for 4 h. Second calcination was done because there is a possibility of lithium escape at higher temperature. So if the compound is formed, this escape can be decreased. Moreover, double calcination makes the powder more homogeneous.

Addition of Al_2O_3 affects the thermal behaviour of these ceramic compositions. It can be seen from the DTA/TG plots that with initial addition of Al_2O_3, the reactivity between the constituent materials increases. It reflects in faster decomposition of Li_2CO_3 at lower temperatures.

4.3.2 Sintering and densification behaviour

Pellets of different batches were sintered at different temperatures ranging from 800 to 925 ^oC for 6 h. The plot of percent relative density with sintering temperature is given in Figure 4.2. At 800 ^oC, with the addition of small amount of Al_2O_3 (x = 0.02), an increase in the relative density by around 9 percent (from 83.00 to 92.39 %) is observed. When the densification behaviour is seen at different sintering temperatures, maximum density is achieved at the sintering temperature of 825 ^oC for all the compositions with Al_2O_3 (x = 0.02 – 0.08). Maximum relative density of 94.13 % is achieved for the composition with x = 0.02 at the sintering temperature of 825 ^oC. For the LMP (x = 0) sample, the densification increases with increase in sintering temperature. It is also reported by Dong et al. (2014c) that pure $LiMgPO_4$ ceramic attains its maximum relative density at 950 ^oC, which is around 95% of the theoretical density.

The addition of small amount of Al_2O_3 (x = 0.02) improves the densification at lower sintering temperature of 825 ^oC. Thus, the optimized sintering temperature is 825 ^oC and all the investigations and material characterizations were performed for the samples sintered at this temperature. The bulk density of LMAP ceramics sintered at different temperatures lies in the range 2.45 – 2.77 g/cm^3 with maximum value of 2.77 for LMAP (x = 0.02) sintered at 825 ^oC (Figure 4.3). The composition with x = 0 does not densify properly at 825 ^oC but for the composition with x = 0.02, density increases. It is worthwhile to mention here that the density of these ceramics is < 3 g/cm^3, thus the

sample is light in weight and the resultant LTCC module fabricated with this material will also be lighter in weight.

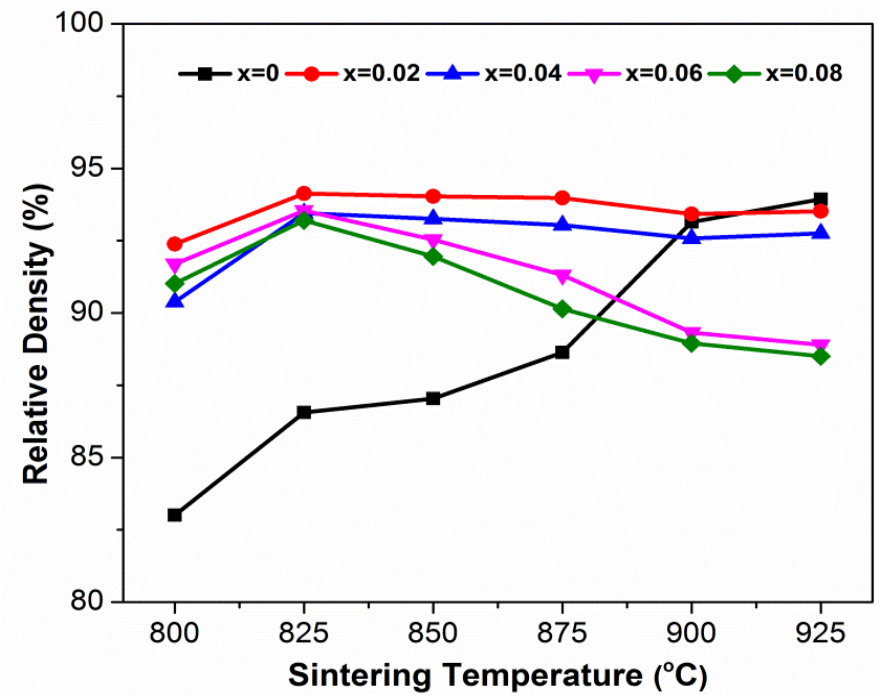

Figure 4.2 Variation of percent relative density of LMAP ceramics at different sintering temperatures.

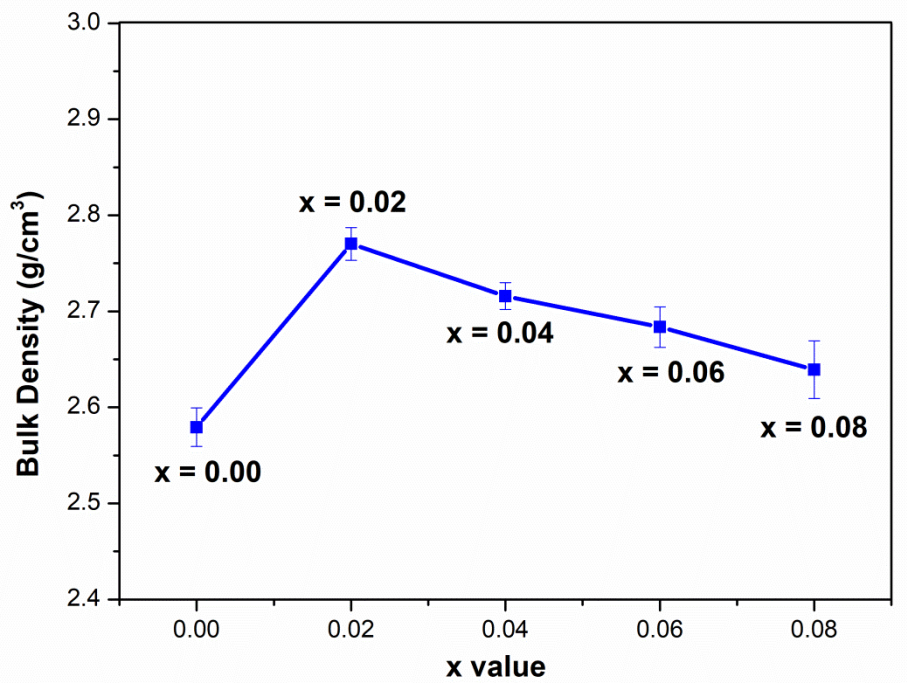

Figure 4.3 Bulk density of LMAP ceramic compositions sintered at 825 ºC.

4.3.3 Phase analysis

Figure 4.4 illustrates the X–ray diffraction (XRD) patterns of Li_2O–(2-3x)MgO–(x)Al_2O_3–P_2O_5 (x = 0.00 – 0.08) ceramics sintered at 825 ^oC for 6 h. Since optimized sintering temperature is 825 ^oC therefore it can be useful for LTCC application. The $LiMgPO_4$ is the major crystal phase identified in the prepared ceramic system. It belongs to Pmnb space group. The peaks of $LiMgPO_4$ (JCPDS file no. 32–0574) are indexed for x=0 in Figure 4.4. $LiMgPO_4$ phase has orthorhombic olivine type crystal structure, which consists of LiO_6 and MgO_6 octahedrons and PO_4 tetrahedrons. Although a few minor peaks of very low intensities of Lithium Phosphate $Li_4P_2O_7$ (JCPDS file no. 13-0440) are also observed in all the samples and marked (#). Li^{1+} and Mg^{2+} occupy distinct sites in $LiMgPO_4$. It is expected that the ions are situated in their respective sites in an ideal lattice. However, due to possible existence of antisite cation exchange in $LiMgPO_4$, some of the divalent cation sites may be replaced by Li ions. These replacements are a point defect in crystal lattices and are called as cation exchange disorder [Menon et al. (2018)]. Kellerman et al. (2018) has also reported the theoretical and experimental evidences of defects in $LiMgPO_4$. With the addition of Al_2O_3 from x = 0.02 to 0.08, another secondary peak of $AlPO_4$ (JCPDS file no. 10-0423) is observed in composition x = 0.04 to 0.08 beside the other common peaks. $AlPO_4$ (α-Berlinite) possesses a hexagonal structure. When x concentration increases, the intensity of $AlPO_4$ peak increases and diphasic composite of $LiMgPO_4$ and $AlPO_4$ forms. It may be due to the large difference in the ionic radii of Al^{3+} and Mg^{2+}. Normally, there is easy replacement of ions in crystal structure with ±15% ionic radii difference. The ionic radii difference between Mg^{2+} and Al^{3+} is around 18.5%. Therefore, the substitution is very much limited in the crystal structure.

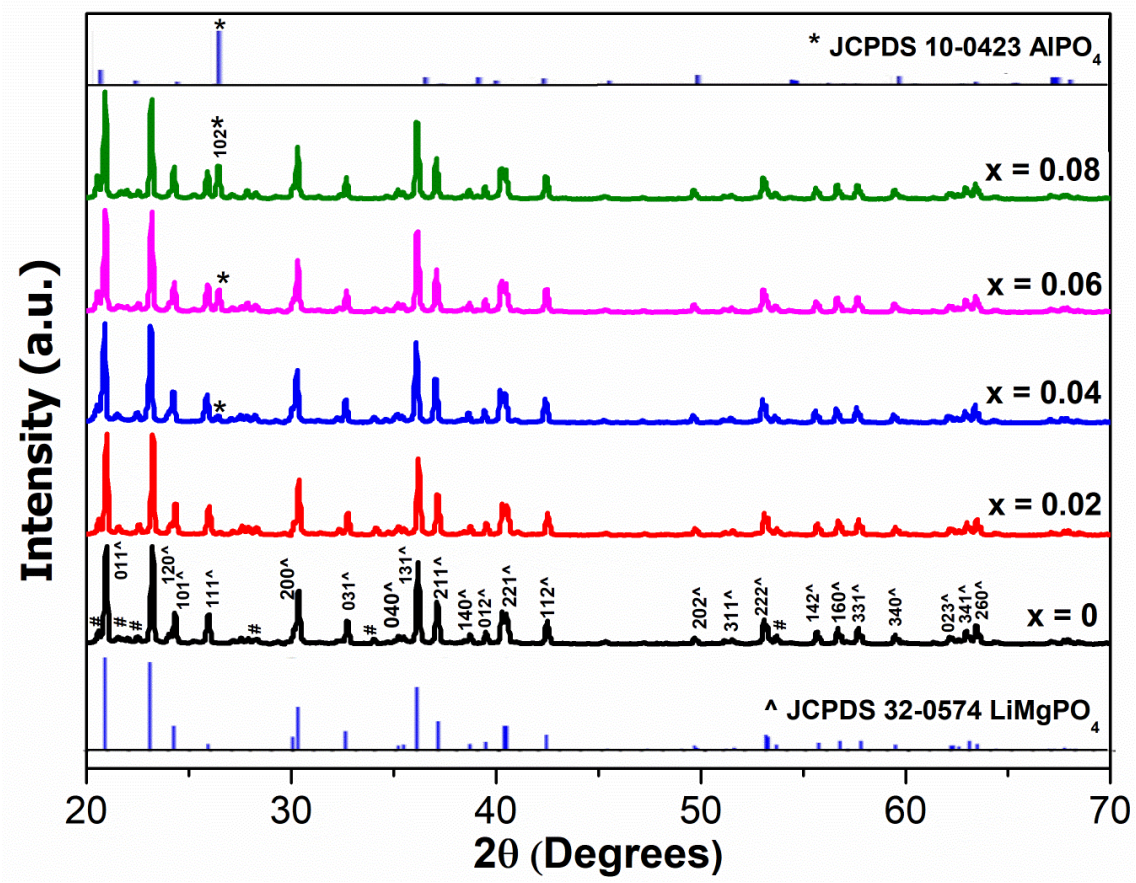

Figure 4.4 XRD patterns of LMAP ceramic compositions.

4.3.4 Microstructure

Figure 4.5 shows the SEM microstructure of all sintered samples at magnification of 5K. The SEM micrograph of the composition with x = 0 (Figure 4.5(a)), shows lower densification on sintering at 825 ^{o}C. Addition of small amount of Al_2O_3 (x = 0.02 – 0.04) results in the bimodal grain distribution as shown in Figure 4.5(b) & 4.5(c). As a result of this bimodal grain distribution, the density has increased. But, by further increasing Al_2O_3 concentration (x > 0.06) led to exaggerated grain growth of some $LiMgPO_4$ crystal, which results in higher porosity in the specimen. The oversized grain can be clearly seen in Figure 4.5(d) & 4.5(e). The presence of secondary $AlPO_4$ crystal in the ceramic matrix,

marked in Figure 4.5(e), is clearly visible for the LMAP (x = 0.08) sample. The SEM micrograph of LMAP (x = 0.02) ceramic with 20 wt% Ag is shown in Figure 4.5(f).

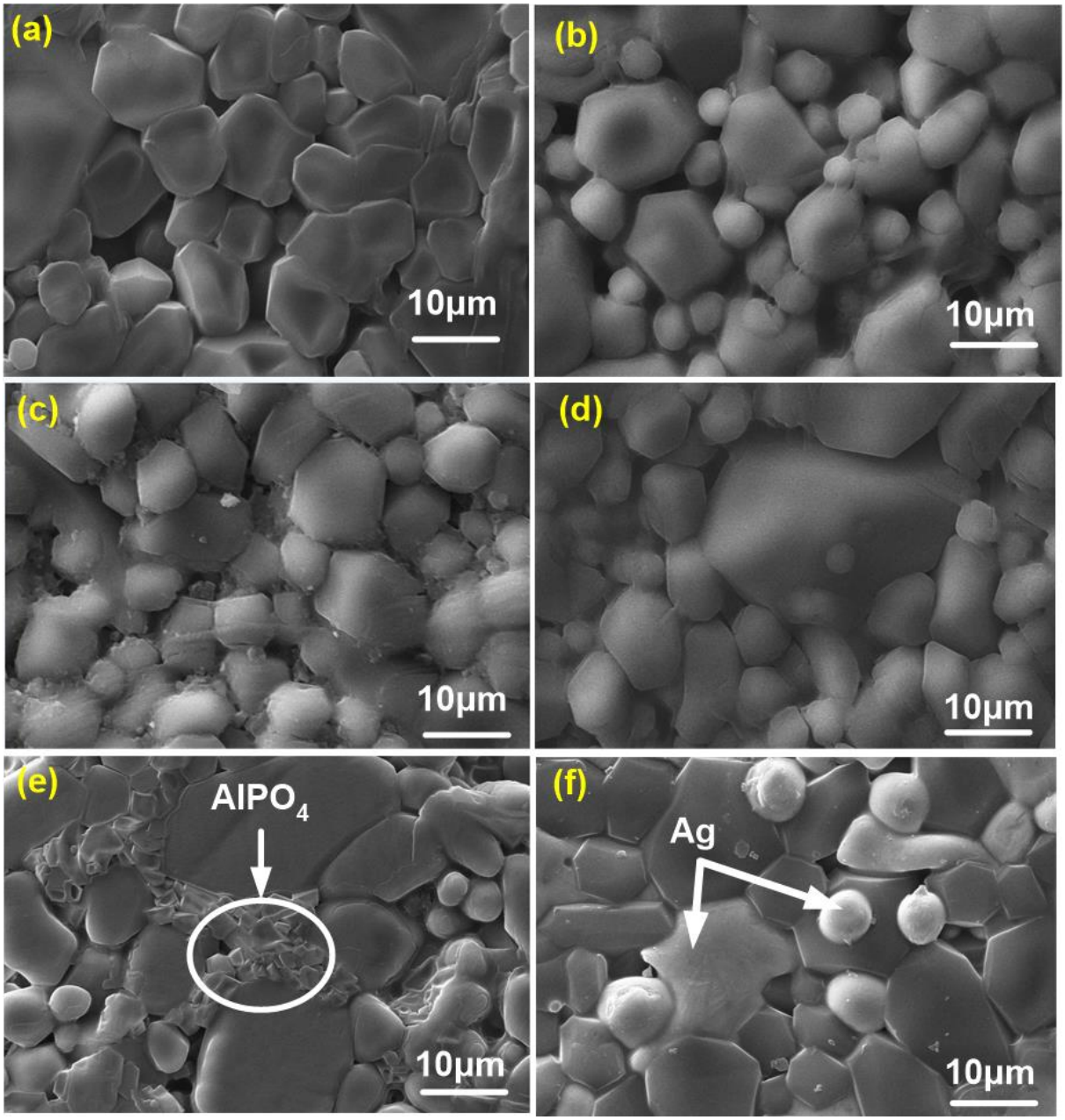

Figure 4.5 The SEM microstructure of LMAP ceramics (a) x = 0, (b) x = 0.02, (c) x = 0.04, (d) x = 0.06, (e) x = 0.08 and, (f) back scattered image of LMAP (x=0.02) with 20 wt% Ag

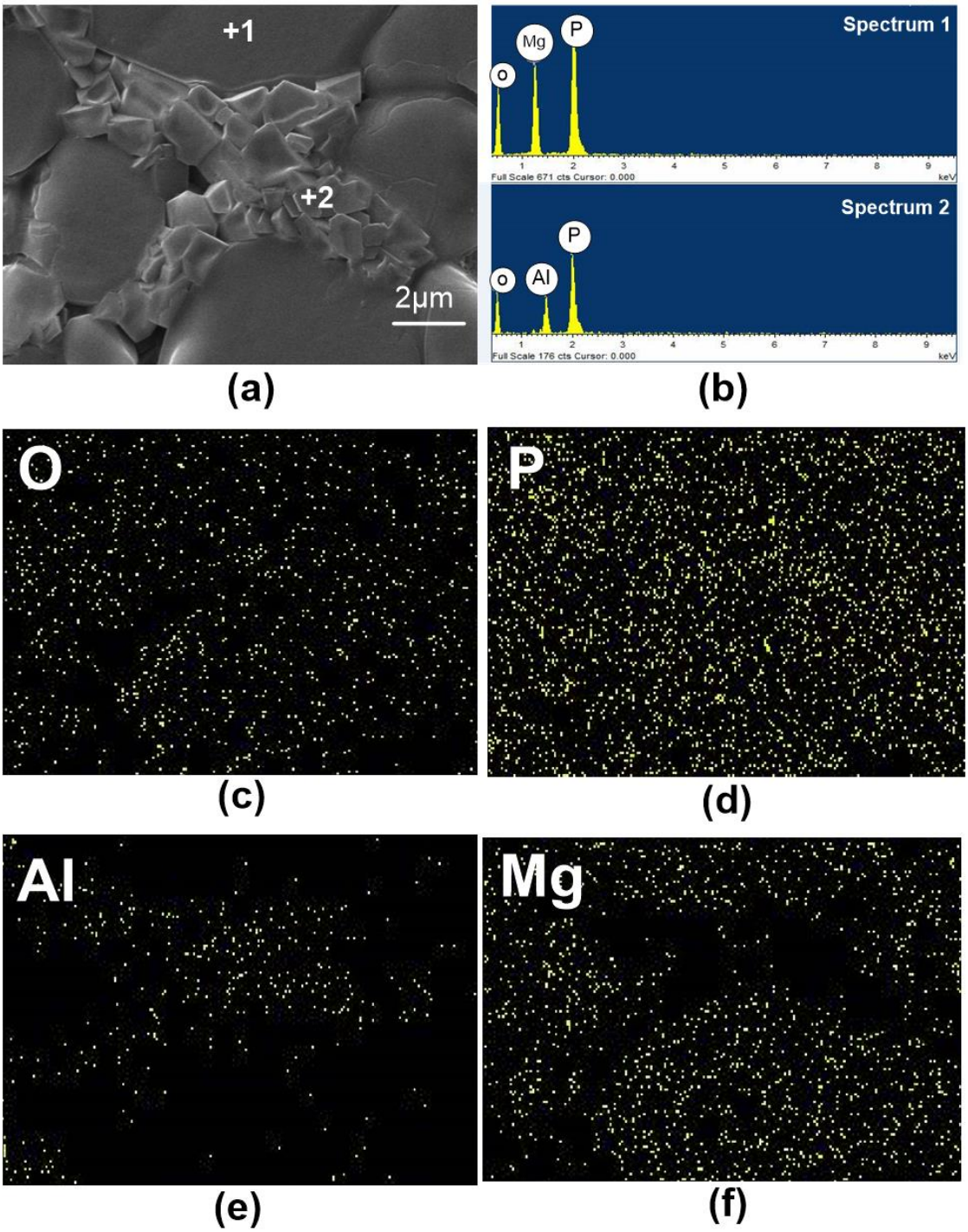

Figure 4.6 SEM/EDS spectra and elemental mapping of $Li_2O-(1.76)MgO-(0.08)Al_2O_3-P_2O_5$ceramics sintered at 825°C, showing the presence of $AlPO_4$ crystals.

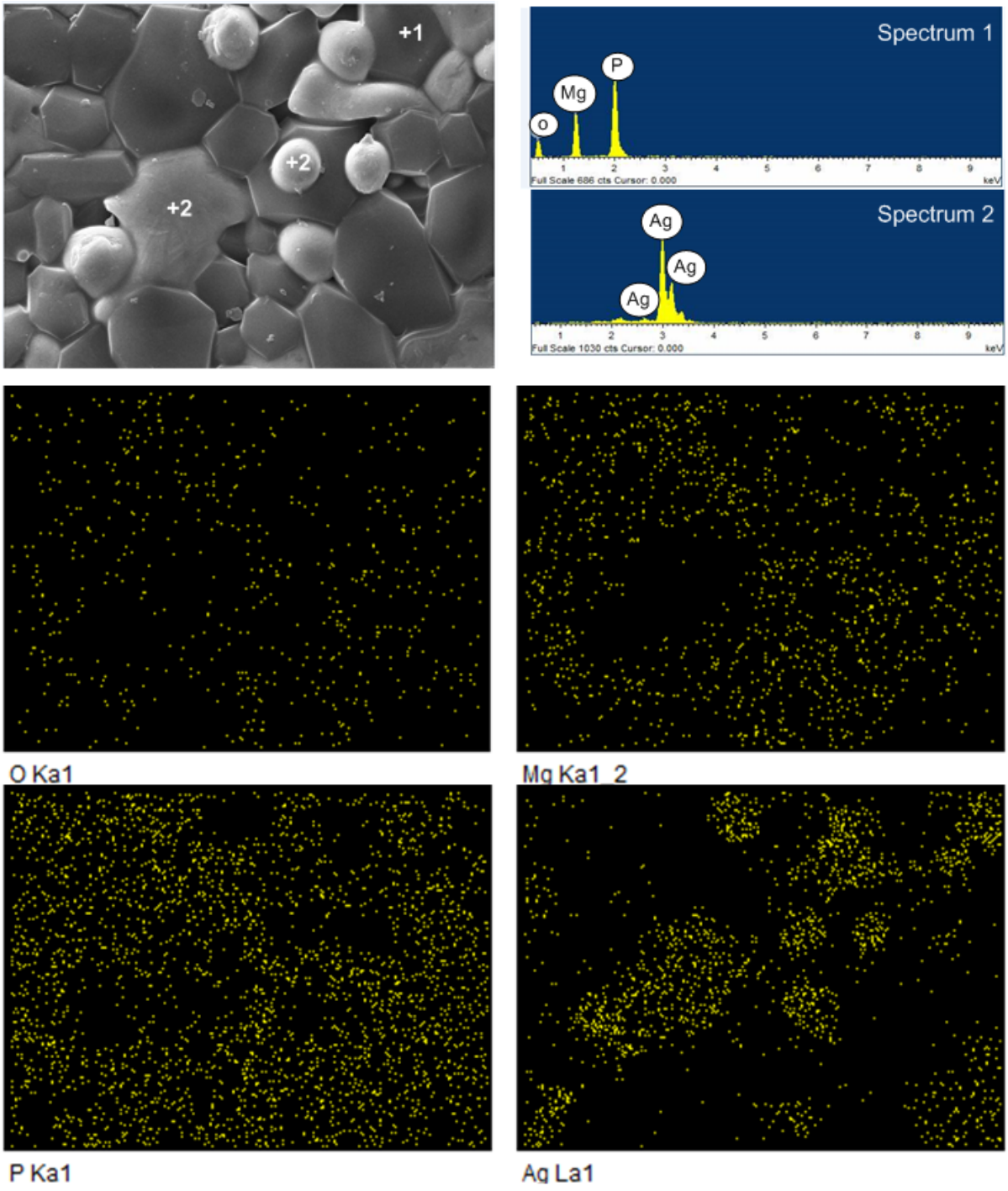

Figure 4.7 SEM/EDS and elemental mapping of the LMAP (x=0.02) ceramic with 20 wt% Ag.

In Figure 4.6, EDS analysis and mapping of Al, P, O and Mg ions in the LMAP (x = 0.08) is shown. Figure 4.6(a) shows the SEM microstructure of LMAP composition with x = 0.08 at magnification of 10K. Lithium, being the light element does not get detected in the EDS spectrum while the presence of magnesium, phosphorus, aluminium and oxygen is visible in the EDS spectrum (Figure 4.6(b)). The elemental mapping of oxygen and phosphorus is homogeneous at all the places in the sample as shown in Figure 4.6(c) and 4.6(d) respectively. In $AlPO_4$, magnesium is absent and in $LiMgPO_4$, aluminium is absent. So, when the elemental distribution of aluminium and magnesium are recorded as in Figure 4.6(e) & 4.6(f) respectively, elemental mapping shows the absence of magnesium where small crystallites of $AlPO_4$ are visible. The presence of $AlPO_4$ in the ceramic matrix is confirmed by XRD but $AlPO_4$ crystallites are not very clearly seen at lower x values (up to 0.06) in SEM micrographs. It is clearly seen in Figure 4.6(a) that a chain or cluster of $AlPO_4$ crystals (1-2μm) form along with the large $LiMgPO_4$ grains in LMAP (x = 0.08) ceramics. Thus it can be concluded that small addition of Al_2O_3 (x = 0.02 – 0.04), enhances the density of the ceramic matrix because of the partial dissolution of Al_2O_3 in the matrix. Further increase in Al_2O_3 content (x = 0.06 – 0.08) results in exaggerated grain growth and also formation of secondary $AlPO_4$ phase.

Silver compatibility test was also performed. The LMAP (x = 0.02) ceramic mixed with 20 wt. % Ag is sintered at 825 ^oC. SEM/EDS and elemental mapping of the as sintered pellet was done for LMAP (x = 0.02) with 20 wt% Ag (Figure 4.7) and it was observed that the ceramic has not reacted with the silver and thus it can be utilised as the electrode material in electronic device applications.

4.3.5 Dilatometry

Figure 4.8(a-e) shows the variation of percent linear thermal expansion of the LMAP ceramics as a function of temperature up to 550 ^{o}C. The thermal expansion behaviour of ceramic materials depends on its crystal structure and bond strength. Ceramics with low coefficient of thermal expansion (CTE) show high bond strength. For all the compositions, the thermal expansion curve was found to be linear. No significant difference in thermal expansion is observed with the different Al_2O_3 concentrations. The CTE of all LMAP compositions lie in between 10.69 – 11.01 ppm/^{o}C. The CTE of LMAP (x = 0.02) ceramic is 10.98 ppm/^{o}C up to 550 ^{o}C.

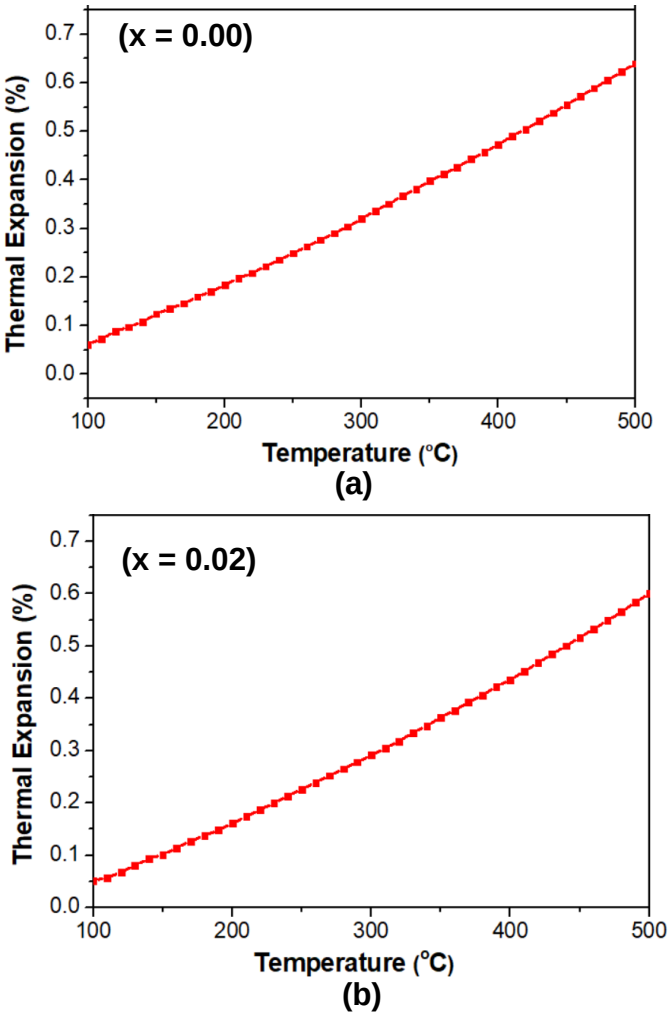

Figure 4.8 Thermal expansion characteristics of LMAP ceramic sintered at 825 ^{o}C (a) x = 0.00 and (b) x = 0.02.

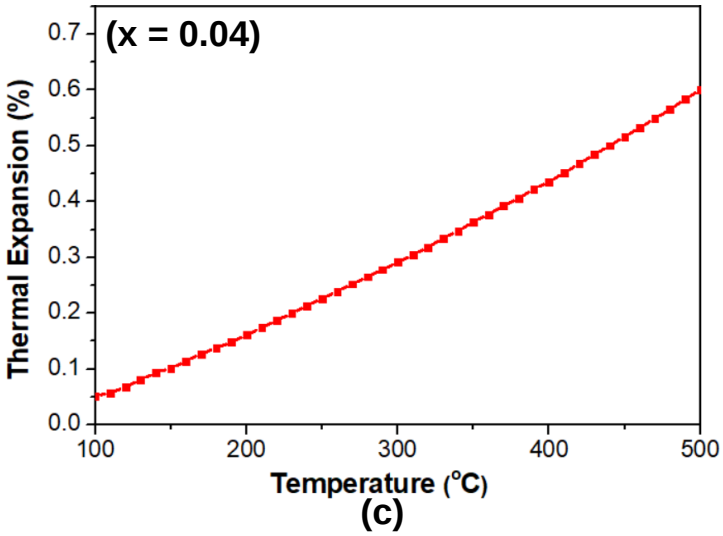

(c)

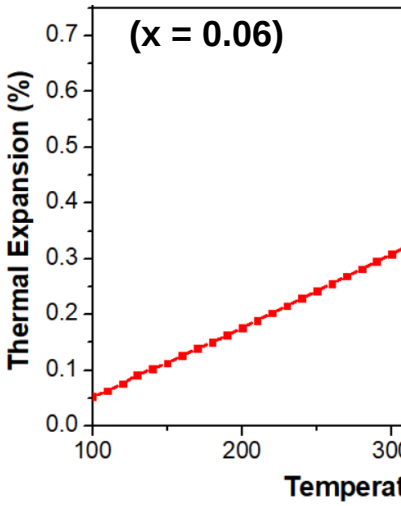

(d

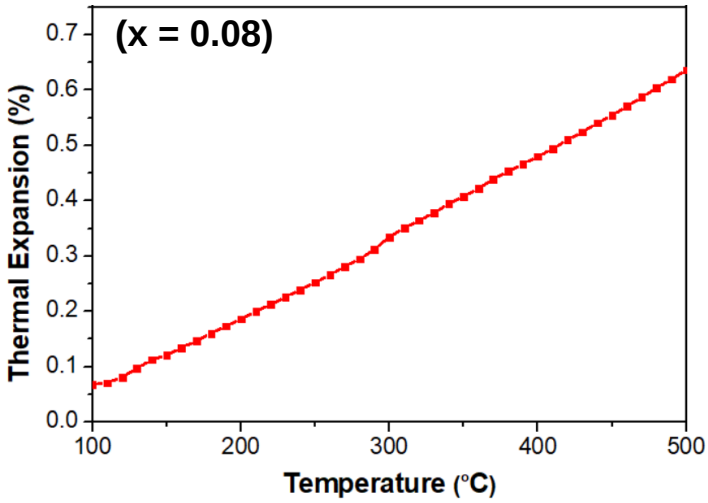

(e)

Figure 4.8 (contd.) Thermal expansion characteristics of LMAP ceramic sintered at 825 ºC (c) x = 0.04, (d) x = 0.06 and (e) x = 0.07.

4.3.6 Thermal conductivity

Thermal conductivity is an important parameter for the substrate application particularly for high power applications where the system failure occurs due to thermal breakdown. So, for these type of applications the material should possess good thermal conductivity. Most of the commercially available substrates possess low thermal conductivity in the range of 2.0 – 4.5 $Wm^{-1}K^{-1}$ [Sebastian and Jantunen (2008b)]. Although, alumina ceramic has high thermal conductivity, but it has high sintering temperature as well. In the present case, the LMAP ceramics possess thermal conductivity in the range 3.0 – 3.8 $Wm^{-1}K^{-1}$. The thermal conductivity of these compositions are listed in Table 4.7.

4.3.7 Dielectric characterization

There is a direct correlation of dielectric constant with the density of the material. If the density is higher, the dielectric constant will also be higher. Therefore, the dielectric constant of around 5 is observed for the LMAP (x = 0) ceramic sintered at 825 ^oC, which consists of majorly $LiMgPO_4$ phase. Had it been sintered at 925 ^oC or above, it would have shown higher densification and greater dielectric constant (> 6) [Dong et al. (2014c); Sebastian (2008a)]. But in case of composition with x = 0.06 to 0.08, the dielectric constant value decreases due to the formation of low dielectric constant $AlPO_4$ and increased porosity. The $AlPO_4$-5 wt% MgF_2 composite sintered at 1450 ^oC shows good microwave dielectric properties (ε_r = 3.0 and $\tan\delta = 7 \times 10^{-3}$) [Abhilash et al. (2013); Sebastian et al. (2015)]. The values of ε_r for different ceramic compositions lie within the range 5.0 – 6.2 (Figure 4.9). It is to be noted that the value of ε_r for LMAP ceramic having x = 0.02 is found to be 6.2. Loss tangent values of these ceramic compositions lie in the order of 10^{-4} (0.0006 – 0.0008) in X– Band. Again it is worthwhile to mention here that LMAP ceramic has loss tangent of 0.0006 for x = 0.02. The materials with low ε_r and low-loss find several applications in microwave engineering for reduction in RC signal

delay and are in constant demand. Low relative permittivity also decreases power consumption and reduces cross-talk [Sebastian and Jantunen (2008b)]. Optimisation in permittivity can be achieved through the control of density by addition of Al_2O_3 in the LMAP ceramics keeping in mind that the device must possess good mechanical, chemical and thermal stability. LMAP ceramic show good dielectric properties in X– Band of microwave frequencies. For different ceramic compositions, the temperature coefficient of resonant frequency (τ_f) for different LMAP compositions lies in the range –63 to –68, similar to the other $LiMgPO_4$ based ceramics (Table 4.8).

Table 4.7 Thermal conductivity of LMAP ceramics at room temperature.

x value	**Thermal conductivity ($Wm^{-1}K^{-1}$)**
0.00	3.027
0.02	3.817
0.04	3.528
0.06	3.312
0.08	3.130

Table 4.8 τ_f values of different LMAP compositions

x value	**TCF (~30 – 70 °C)**
0.00	-65
0.02	-63
0.04	-64
0.06	-68
0.08	-68

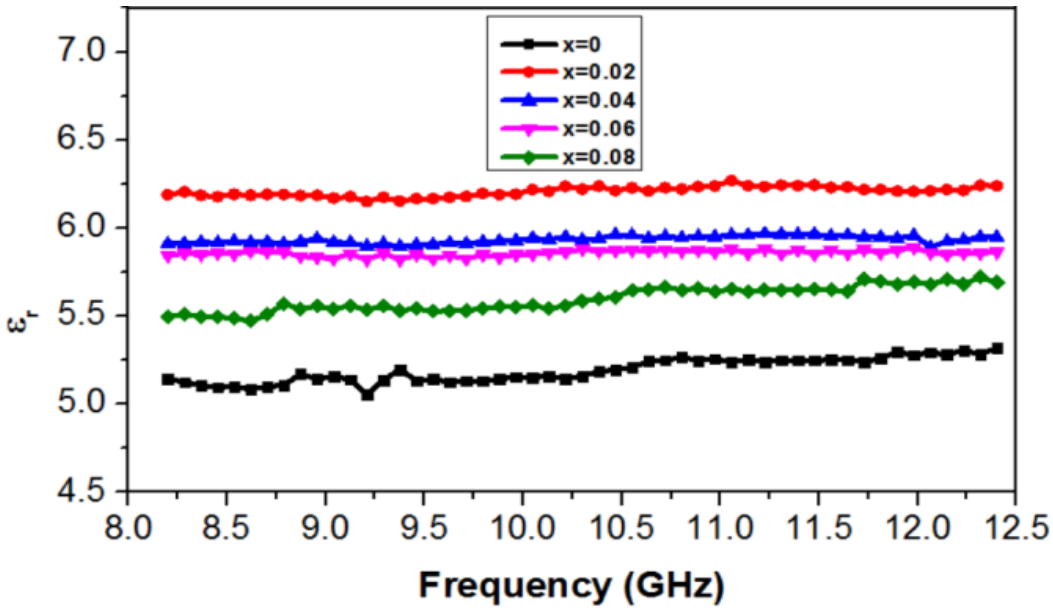

Figure 4.9 The variation of relative permittivity ε_r of LMAP ceramics with frequency.

4.4 Summary

Li_2O–(2-3x)MgO–(x)Al_2O_3–P_2O_5 (LMAP) (x = 0.00 – 0.08) ceramic system was prepared through solid state synthesis route at different sintering temperatures (800 – 925 ^oC). A small addition of Al_2O_3 (x = 0.02) in LMAP ceramics lowers the sintering temperature by more than 100 ^oC with good relative density of 94.13 %. The sintered samples were characterized in terms of thermal behaviour, density, phase, micro-structure and microwave dielectric properties. Silver compatibility test is also performed for its use as electrode material in LTCC application.

The LMAP ceramic has been found to have good structural and microwave dielectric characteristics. From the XRD analysis, it has been observed that LMAP ceramic majorly consists of $LiMgPO_4$ phase. The $AlPO_4$ crystallites have been observed in the SEM micrograph for the case of ceramic composition with x = 0.08. Dielectric constant for LMAP ceramics with different values of x lies in the range 5.0 – 6.2 in X– band (8.2 – 12.4 GHz). It is concluded that the proposed material can be used as LTCC substrate

material in realization of low loss microwave components and dielectric resonator antennas for radar, radio navigation, radio astronomy and satellite communication.

In the next Chapter 5, the prepared LMAP is utilised as substrate for the investigation of a microstrip–fed aperture–coupled dual segment cylindrical dielectric resonator antenna (DS-CDRA). Further, this ceramic is also utilised as component of resonating material for the design of 4–element composite triangular dielectric resonator antenna (4–CTDRA) described in Chapter 6.